J. Electrochem. Sci. Eng. **4(3)** (2014) 97-110; doi: **10.5599/jese.2014.0063**

Open Access: ISSN 1847-9286

www.jESE-online.org

Original scientific paper

The effect of cetyltrimethylammonium bromide on size and morphology of ZnO and CuO

Anantha N. Subba Rao, Venkatesha T. Venkatarangaiah✉

Department of P.G. studies and Research in Chemistry, School of Chemical Sciences, Kuvempu University, Shankaraghatta-577451, Karnataka, India

✉*Corresponding author: E-mail: drtvvenkatesha@yahoo.co.uk, Tel.: +91-9448855079; fax: +91-08282-256255*

Received: April 1, 2014; Revised: September 15, 2014; Published: September 22, 2014

Abstract

The nanoparticles (NP) ZnO and CuO were synthesized by electrochemical-thermal method. The influence of cetyltrimethylammonium bromide (CTAB) on size and morphology of NP was evaluated. They were characterized by powder X-ray diffraction spectroscopy (XRD), scanning electron microscopy (SEM), UV-Visible absorption spectroscopy. The average crystallite size and the average grain size of NP decreased with CTAB concentration. The CTAB significantly affected the morphology of CuO and ZnO NP. The regular spindle shape of CuO transformed into irregular spherical shape and the homogeneity in the morphology of spherical ZnO NP was lost with increase in CTAB concentration. The effect of morphology and size of ZnO on its photocatalytic activity was evaluated by subjecting methylene blue (MB) dye to photocatalytic degradation under the irradiation of UV light. The color removal of MB dye during electrolysis was monitored by UV-Visible spectroscopy. The highest photocatalytic activity was noticed for ZnO 10 mM CTAB.

Keywords

Electrolysis; Photocatalyst; Morphology; Methylene blue; Degradation; Surfactant; Nanoparticles; Color removal; Absorbance; Band gap

Introduction

The TiO_2, SnO_2, Fe_2O_3, PdO, WO_3, Ga_2O_3, In_2O_3, ZrO_2, CuO and ZnO are amongst the extensively studied transition metal-oxide semiconducting nanomaterials and have potential applications in optics, optoelectronics, microelectronics, biosensors, gas sensors, chemical sensors, switching, magnetic, luminescent, electrical and acoustic devices, solar cells, catalysis and powder metal-

lurgy [1-4,5]. The CuO and ZnO nanomaterials are particularly of special interest as they are cheap, easy to prepare by simple, low cost methods at normal temperatures [6]. They exhibit diverse nanostructure configurations and show superior performance in many applications.

CuO is a p-type semiconductor with band gap of 1.8 to 2.5 eV [2,7]. It is an excellent solar absorber with low emittance, which makes it a suitable candidate for solar cells as thermal collector [8]. The suspension of CuO NPs in the heating or cooling fluids substantially increases the thermal conductivity [9]. CuO is highly responsive in non-enzymatic glucose sensing and H_2S gas sensing [1,10-12]. CuO on ceria shows high catalytic activity for the oxidation of NO, CO and dehydrogenolysis of CH_4 [13].

ZnO on the other hand, is extensively studied and widely recognized for its photocatalytic activity. ZnO, with a high surface reactivity owing to large number of active sites, has emerged to be an efficient photocatalyst [14,6]. The nanocrystalline ZnO is non-toxic and has the ability to kill or restrain bacteria [4]. It has a wide band gap of 3.2 eV and large exciton binding energy of 60 meV, which makes it a preferable material in low-voltage and short wavelength optoelectronic devices such as light emitting diodes and diode lasers [5]. The applicability of ZnO is widening with the extending knowledge of its physico-chemical properties. ZnO nanomaterials are also used in solar cells, luminescent, electrical and acoustic devices, chemical sensors, catalysis, electronics, gas sensor devices, optoelectronics, transducers [3,4].

The synthesis of ZnO and CuO thus acquires special interest. The common chemical synthetic methods adopted in the preparation of these nanomaterials are precipitation, sol-gel, hydrothermal, solvothermal, solution combustion, thermal decomposition, simple hydrolysis, wet-chemical, microemulsion, non-microemulsion, microwave assisted solvothermal, ultrasonic radiation precipitation, mechanical milling, electrochemical, chemical vapor deposition (CVD), laser vaporization, exfoliation, laser ablation methods and so on [2]. However, these methods involve organic solvents, rigorous reaction conditions, demand sophisticated instruments and few of these techniques require longer time duration affording less yield than expected [4].

The organic solvents can be replaced completely with aqueous medium using electrochemical method. Electrochemical method is fast, cheap, and easy to control and provides appreciable yields even at normal temperature and mild conditions. It was Reetz and co-workers who proposed the sacrificial anode electrochemical route for the synthesis of nano metal clusters and colloids and showed that it is possible to control the particle size by adjusting the applied current density [15-17]. Gao-Qing *et al.* demonstrated that the size and shape of the synthesized CuO nanocrystals could be controlled by changing the solvent system [12]. Mahamuni and co-workers prepared ZnO quantum dots using the sacrificial anode electrochemical method [18]. The ZnO [19], Cu_2O [20], CuO [21], Au/AgI [22] have been successfully synthesized by electrochemical method. We have recently synthesized hexagonal shaped CuO NP in bulk [2], cubic shaped Zn_2SO_4 [23] and large size ZnO NP [3,4] by hybrid sacrificial anode electrochemical-thermal route.

There are many factors to be monitored in the electrochemical synthesis to control the size and shape of NPs. The current density, distance between the electrodes, solvent system, temperature, supporting electrolyte and stabilizing agent are the most critical parameters which dictate the size and morphology of resulting NPs. The role of stabilizing agent is to bind to the surface of NP, decrease the surface energy, control growth and shape evolution and prevent the agglomeration of NPs [24]. Cetyl trimethylammonium bromide (CTAB) a cationic surfactant is the most commonly used stabilizing agent in controlling the shape and size of NPs [24-29]. Oscar *et al.* [24] reported that in the synthesis of gold nanorods, CTAB dictates the crystal growth along the faces by binding

to the surfaces along the sides of nanorod. Reetz and co-workers have demonstrated the role of surfactant (CTAB) in the formation of nanoclusters and nanocolloids [15-17]. In this paper, we have systematically studied the effect of CTAB concentration in the electrolyte bath, on the morphology and size of ZnO and CuO metal oxide NPs prepared by hybrid sacrificial anode electrochemical-thermal route. Furthermore, the photocatalytic degradation of methylene blue dye on ZnO NP was studied in order to evaluate the effect of size and shape of the NPs on its photocatalytic activity.

Experimental procedure

Materials and synthesis of ZnO and CuO NP

Zinc and copper metal plates (99.99 % pure) were purchased from Sisco research laboratories, Mumbai. AR grade $NaHCO_3$, $NaNO_3$, CTAB and methylene blue (MB) dye purchased from S. D Fine Chemicals Ltd. India, were used without further purification. The electrolyte solution was prepared in Millipore water (specific resistance > 18 MΩ at 25 °C, Millipore Elix 3 water purification system, France). The electrolysis was carried out under constant current supply from potentiostat / galvanostat source (Model PS-618 chemilink systems, Navi Mumbai, India).

The experimental procedure for the electrochemical-thermal synthesis of ZnO NP was followed as mentioned in our previous work [4]. The two Zn metal plates with dimension 4 x 4 x 0.1 cm^3, were dipped in 1 M HCl for 30 seconds and washed thoroughly with Millipore water. These plates were then immersed in a rectangular electrolytic glass cell containing 250 cm^3 of 60 mM $NaHCO_3$ with or without CTAB. Three different concentrations of CTAB (5 mM, 10 mM and 15 mM) were used. The NP prepared in presence of 'x' mM concentration of CTAB is hereafter represented as MO/x, where M is Zn or Cu. The distance between the two electrodes was maintained to be 5 cm. The electrolysis was carried out for 90 minutes under constant current density of 4.9 mA cm^{-2} with constant stirring at the rate of 500 rpm. The electrolytic bath temperature was maintained around 26 ± 1 °C. The pH of the electrolytic bath was noted before and after electrolysis. The resulting colloidal solution was filtered and the solid residue thus obtained was calcined at 300 °C for 1 hour. The same procedure was followed in the preparation of CuO NP, except that the electrodes were pretreated Cu plates and the electrolyte was 60 mM $NaNO_3$. As a pretreatment, the Cu metal plates were dipped in 5 % HNO_3 for 1 minute.

Characterization of NP

The crystallite size of the NPs was evaluated by powder X-ray diffraction (XRD) pattern using X'pert Pro diffractometer (Phillips, Cu-K_α radiation, λ_{Cu}= 1.5148 Å) working at 30 mA and 40 kV recorded in the 2θ range between 10° and 90° (scan rate 1° min^{-1}). The Scherrer equation was made use in estimating the average crystallite size. The scanning electron microscope (Philips XL 30) fitted with an energy dispersive X-ray (EDAX) analyzer recorded the morphology and composition of the synthesized NP. The band gap of the synthesized NPs was evaluated by the UV-Visible absorption spectrum of solid ZnO and CuO NPs using UV-Visible spectrophotometer (HR 4000 UV-Vis spectrophotometer, UV-Vis-NIR light source, DT-MINI-2-GS, Jaz detector).

Photocatalytic degradation of MB dye

To evaluate the photocatalytic activity of ZnO NP, 50 mg L^{-1} MB dye solution was prepared using Millipore water. 30 mg ZnO nanoparticle was added to 30 mL MB solution and stirred for 2 hours in dark to establish equilibrium between adsorption/desorption of MB on NPs. Then, this

solution was exposed to continuous flash of UV light for duration of 10 minutes. A high pressure mercury vapor lamp (HPML) of 125 W (Phillips, India) was jacketed in a quartz tube provided with inlet and outlet for water circulation to avoid rise in temperature of the solution. The UV-lamp radiated predominantly at 365 nm (3.4 eV) and photon flux of 5.8×10^{-6} mol of photons sec^{-1}. 0.5 mL of the irradiated sample was removed, diluted with 1 mL Millipore water and subjected to centrifugation for 5 minutes. The supernatant liquid was taken for UV-Visible spectroscopic analysis. After 2 minutes, the UV light irradiation was again continued for 10 minutes and then sample was removed. The total time of UV light irradiation on the sample was 60 minutes.

Results

XRD analysis

The XRD patterns obtained for ZnO NPs prepared in presence of different concentrations of CTAB are given in Fig. 1.

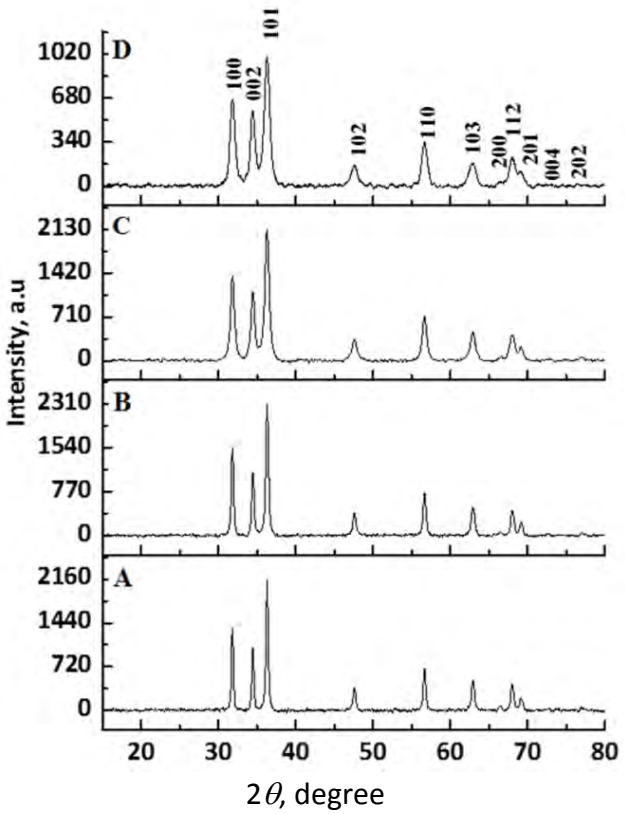

Figure 1. *The XRD pattern of A) ZnO/0; B) ZnO/5; C) ZnO/10; D) ZnO/15*

The positions and intensities of the diffraction peaks of ZnO NPs are in good agreement with the literature values of hexagonal phase ZnO (JCPDS card No. 36-1451) with primitive lattice structure. The crystallite size of the NPs was calculated from full wave half maximum intensity (FWHM) of each peak using Scherrer's formula and the average crystallite size was determined.

$$D = \frac{K\,\lambda}{\beta\cos\theta}$$

In the above formula, *D* is the diameter of the crystallite size, *K* - the shape factor (the typical value is 0.9), λ - the wavelength of the incident beam, β - the broadening of the diffraction line measured in radians at FWHM and θ is the Bragg's angle. The crystallite size of ZnO NPs calculated using the XRD data is given in Table 1.

Table 1. *The average crystallite size of ZnO NPs prepared in presence of CTAB*

Zinc oxide NP	Crystallite size, nm									
	Family of crystallographic planes {hkl} and corresponding 2θ values									
	{100}	{002}	{101}	{102}	{110}	{103}	{200}	{112}	{201}	Average
	31.8°	34.5°	36.3°	47.6°	56.7°	62.9°	66.4°	68.1°	69.2°	
ZnO/0	44	98	45	28	106	55	23	40	47	**48**
ZnO/5	44	44	41	23	66	27	35	31	24	**34**
ZnO/10	25	31	23	16	39	18	24	21	24	**23**
ZnO/15	16	20	27	13	11	20	23	20	24	**18**

The crystallite size of NP markedly decreased with increase in concentration of CTAB in the electrolyte bath. The width of the peaks appreciably increased suggesting the reduction in the crystallinity of ZnO with increase in CTAB concentration.

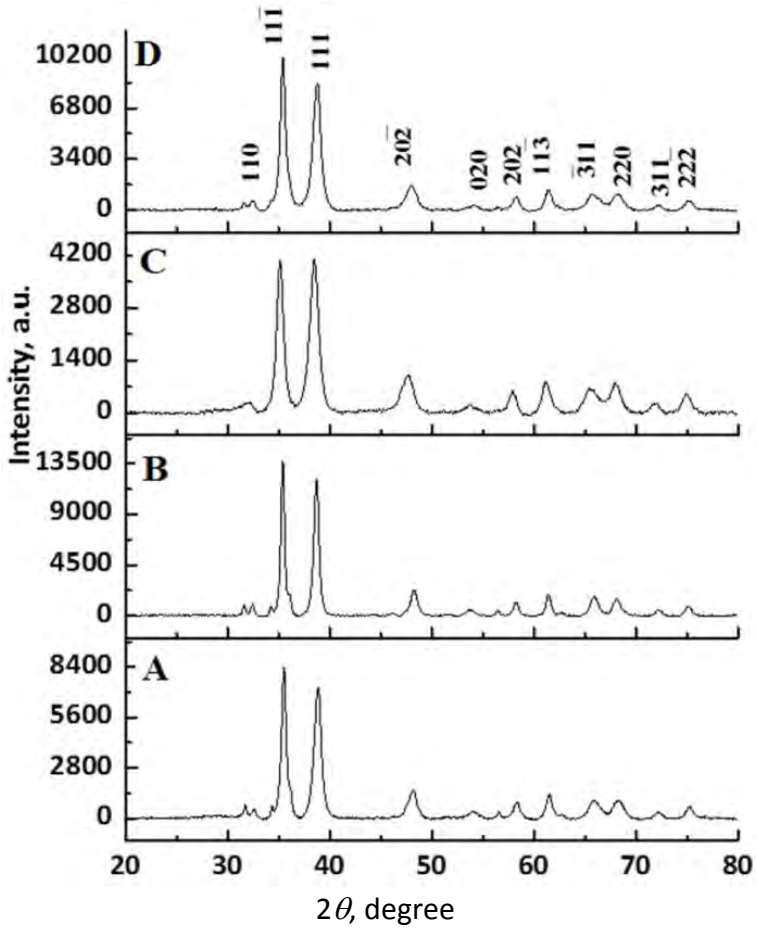

Figure 2. *The XRD pattern of A) CuO/0; B) CuO/5; C) CuO/10; D) CuO/15*

The XRD patterns of synthesized CuO (Fig. 2) are in close match with the XRD pattern of JCPDS card no. 48-1548 with monoclinic (tenorite) phase crystallite structure. The crystallite size of CuO NPs calculated using the XRD data is given in Table 2. The crystallite size of CuO NPs also decreased with increase in CTAB concentration.

Table 2. *The average crystallite size of CuO NP prepared in presence of CTAB.*

Copper oxide NP	Crystallite size, nm											
	Family of crystallographic planes {hkl} and corresponding 2θ values											
	{110}	{111}	{111}	{202}	{020}	{202}	{113}	{311}	{220}	{311}	{222}	**Average**
	32.1°	35.1°	38.5°	47.8°	53.7°	57.9°	61.1°	65.3°	68.1°	71.9°	74.9°	
CuO/0	22	49	44	14	15	24	24	25	11	22	18	**31**
CuO/5	36	26	36	16	14	20	20	20	30	26	15	**26**
CuO/10	09	22	22	13	10	24	15	18	18	13	13	**16**
CuO/15	18	33	11	17	16	14	33	17	09	12	22	**19**

SEM/EDAX analysis

The changes in the morphology of ZnO (Fig. 3) and CuO (Fig. 4) NPs with CTAB concentration are evident from the SEM images. From Fig. 3 and Fig. 4, it can be noticed that the change in the morphology of both CuO and ZnO crystals is not obvious within 5 mM CTAB, but the tendency from regular shapes to irregular ones increases with the increase of CTAB concentration.

The spherical shape of ZnO crystals was though retained, the irregularity in the shape increased with increase in CTAB concentration. The shape of CuO crystals changed from nanospindles (Fig. 4A and Fig. 4B) to irregular nanospheres (Fig. 4C and Fig. 4D). Similar changes in the morphology of CuO crystals were observed by Gao-Qing Yuan *et al.* [12] on varying the solvent system. The average grain size of ZnO and CuO NPs as depicted from SEM images is given in Table 3.

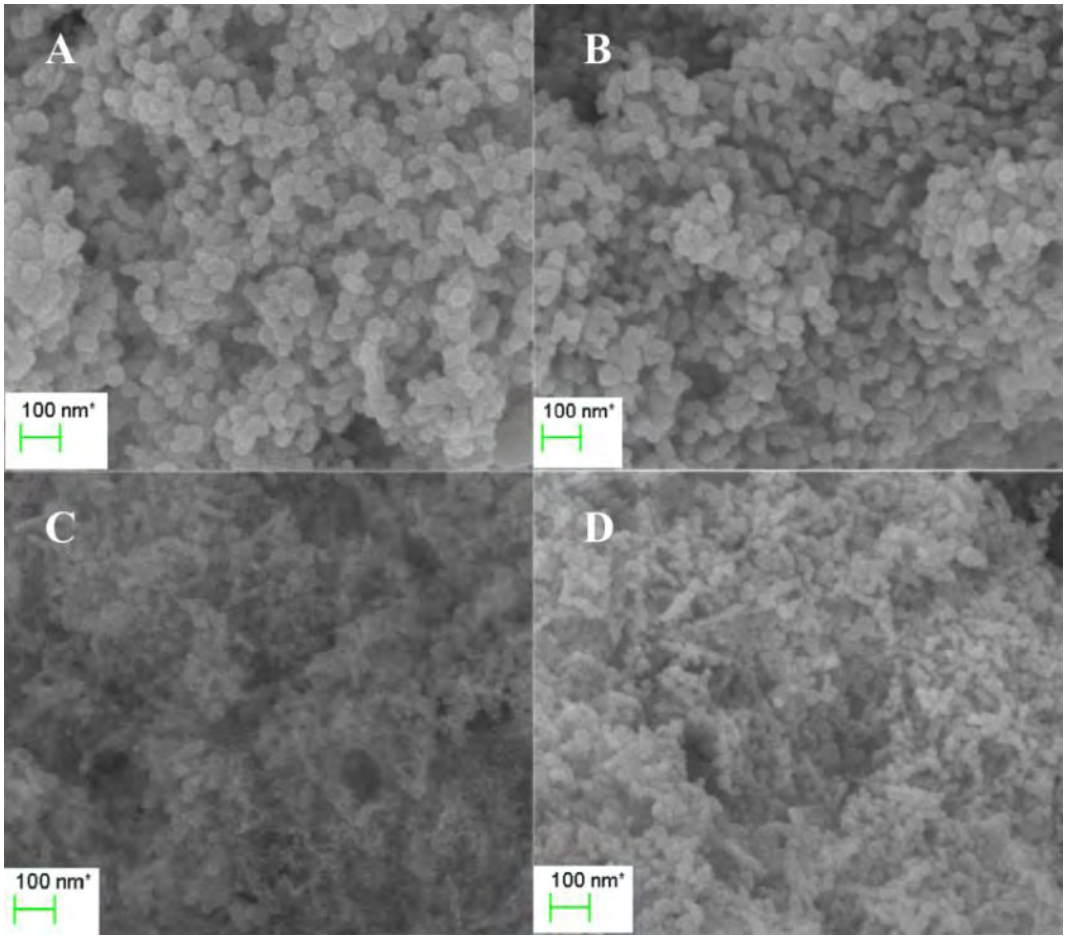

Figure 3. *SEM images of ZnO NP; A) ZnO/0; B) ZnO/5; C) ZnO/10; D) ZnO/15*

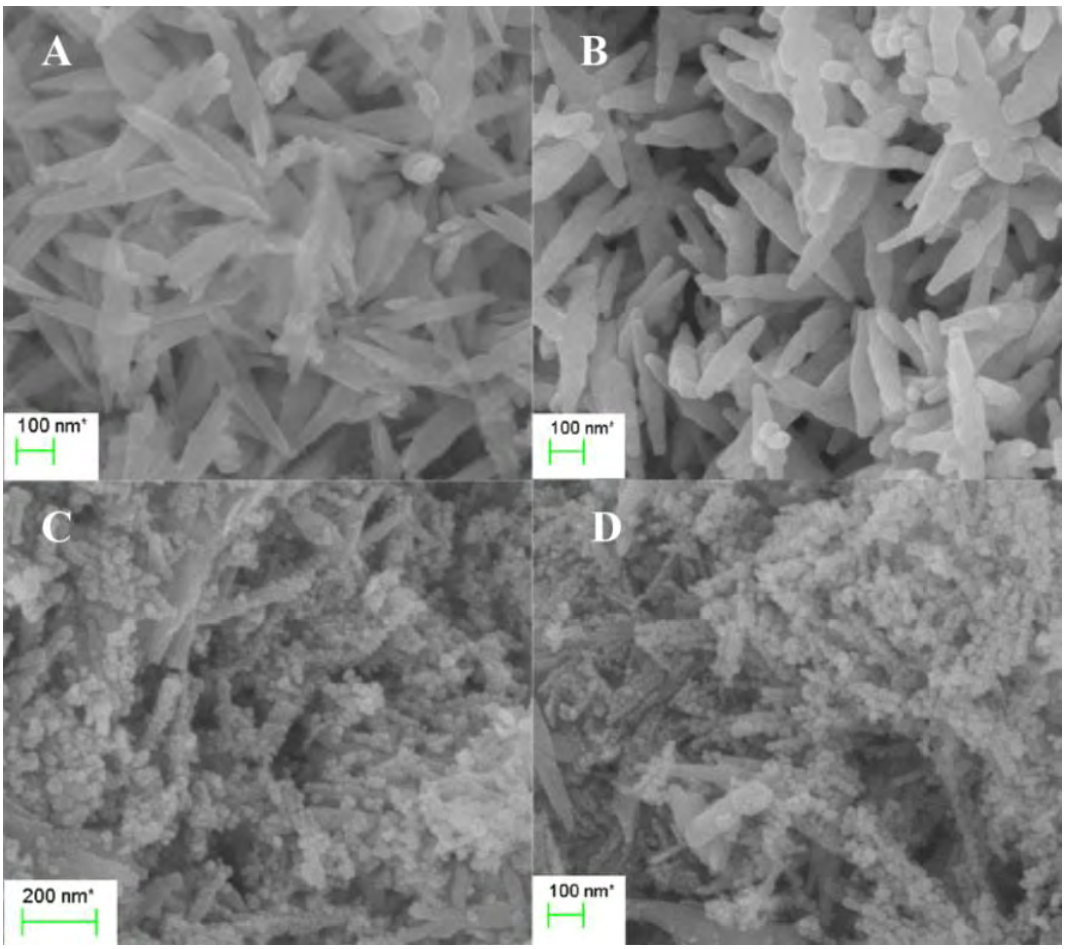

Figure 4. *SEM images of CuO NP; A) CuO/0; B) CuO/5; C) CuO/10; D) CuO/15*

Table 3. *The average grain size of ZnO and CuO NPs prepared in presence of CTAB*

Metal oxide NP	Average grain size, nm			
	0 mM CTAB[a]	5 mM CTAB	10 mM CTAB	15 mM CTAB
ZnO	32-42	31-40	30-69	25-29
CuO	60-65	85-95	18-40	27-64

[a] The CTAB concentration in electrolyte bath

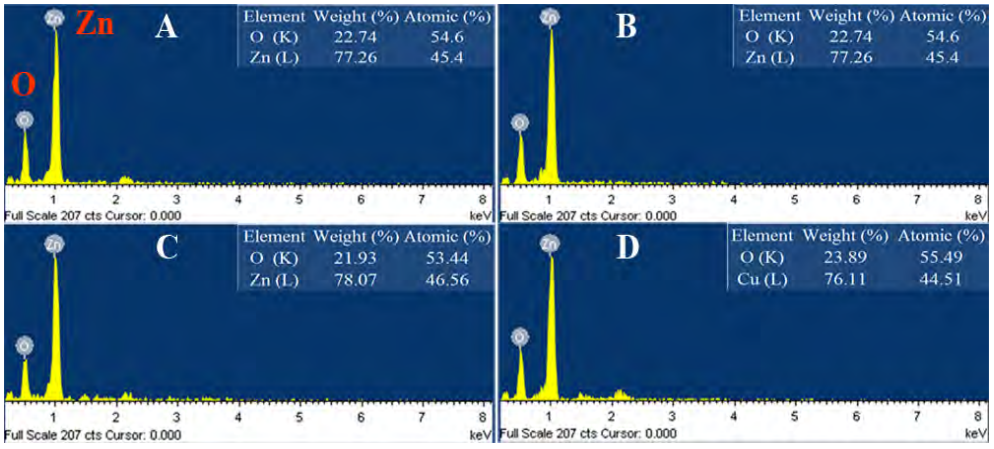

Figure 5. *EDAX analysis of ZnO NP; A) ZnO/0; B) ZnO/5; C) ZnO/10; D) ZnO/15*

The shape and size of CuO/0 and CuO/5 nanospindles was homogeneous. The length of the nanospindles ranged between 430 nm to 580 nm and the rigidity enhanced from CuO/0 to CuO/5.

The CuO/10 and CuO/15 NPs showed irregular morphologies (nanospindle, nanosphere, nanoplate). In case of ZnO NPs, the homogeneity in the spherical shape was lost as the CTAB concentration was increased in the electrolyte bath. There was only slight reduction in the grain size from ZnO/0 to ZnO/15.

The stoichiometry of metal ion and oxygen in the synthesized ZnO and CuO nanomaterials was determined by EDAX analysis (Fig. 5 and Fig. 6). No peaks corresponding to impurities were found suggesting that the synthesized ZnO and CuO nanomaterials are pure.

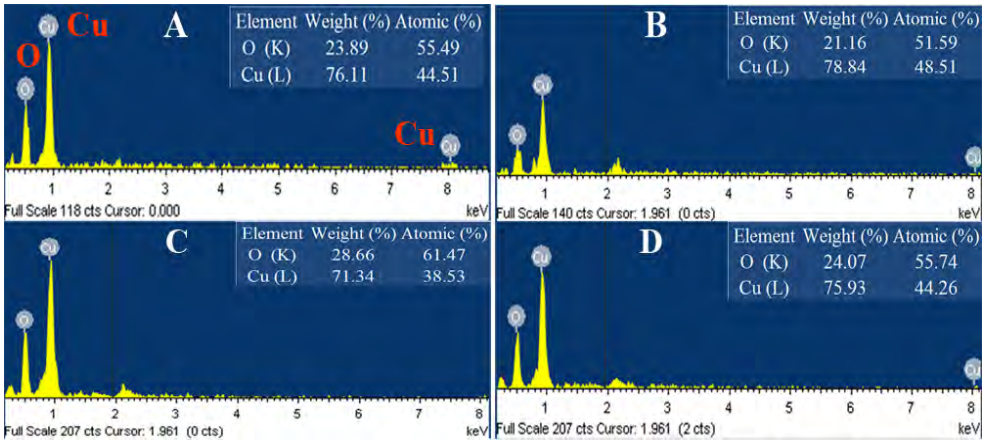

Figure 6. *EDAX analysis of CuO NP; A) CuO/0; B) CuO/5; C) CuO/10; D) CuO/15*

UV-Visible spectroscopy

To better understand the optoelectronic properties of NP, the band gap energy was calculated from their absorption curves using Tauc plots. The UV-Visible absorption spectra of ZnO and CuO NPs are given in Fig. 7A and Fig. 7B respectively. Firstly, the absorption coefficient (α) was calculated using Eq. (1):

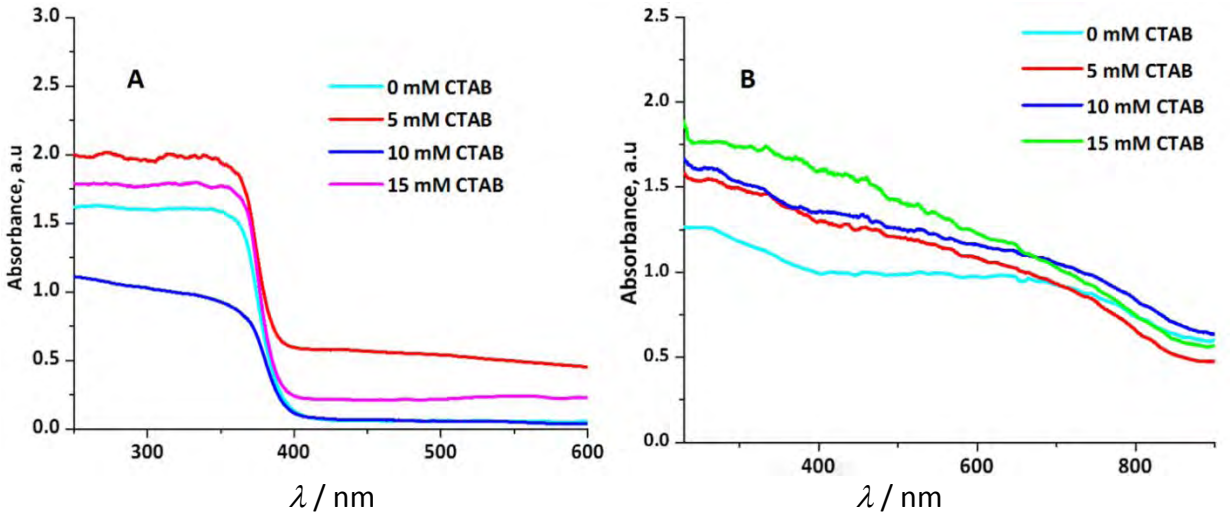

Figure 7. *UV-Visible absorption spectra of A) ZnO NPs and B) CuO NPs synthesized in presence of different concentrations of CTAB*

$$\alpha = \frac{2.303\,A}{d} \qquad (1)$$

where *A* is absorbance, *d* is the thickness of sample. To determine the band gap of NP, a plot of $(\alpha h\nu)^n$ *vs. Eg* was made (Tauc plot). The value of 'n' is dependent on the mode of electronic

transition; n = 2 for direct band transitions and n = 1/2 for indirect transitions. For both ZnO and CuO, it is known that the electronic transition is direct. Therefore, Eq. (2) is valid for both ZnO and CuO NP:

$$(\alpha h\nu)^2 = B\,(h\nu - Eg) \quad (2)$$

where, *B* is a constant, *hν* is the photonic energy. The band gap (*Eg*) was obtained by extrapolating the linear part of the graphics to the axis of the abscissa [30].

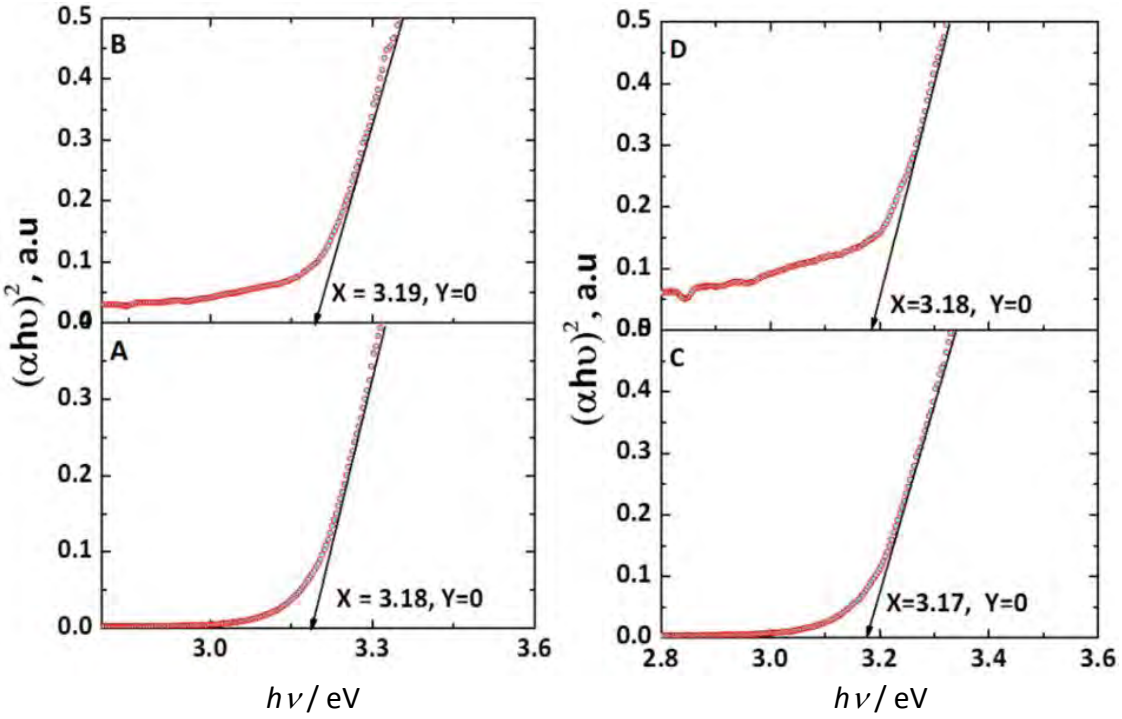

Figure 8. *Tauc plots for the evaluation of band gap of samples A) ZnO/0; B) ZnO/5; C) ZnO/10; D) ZnO/15*

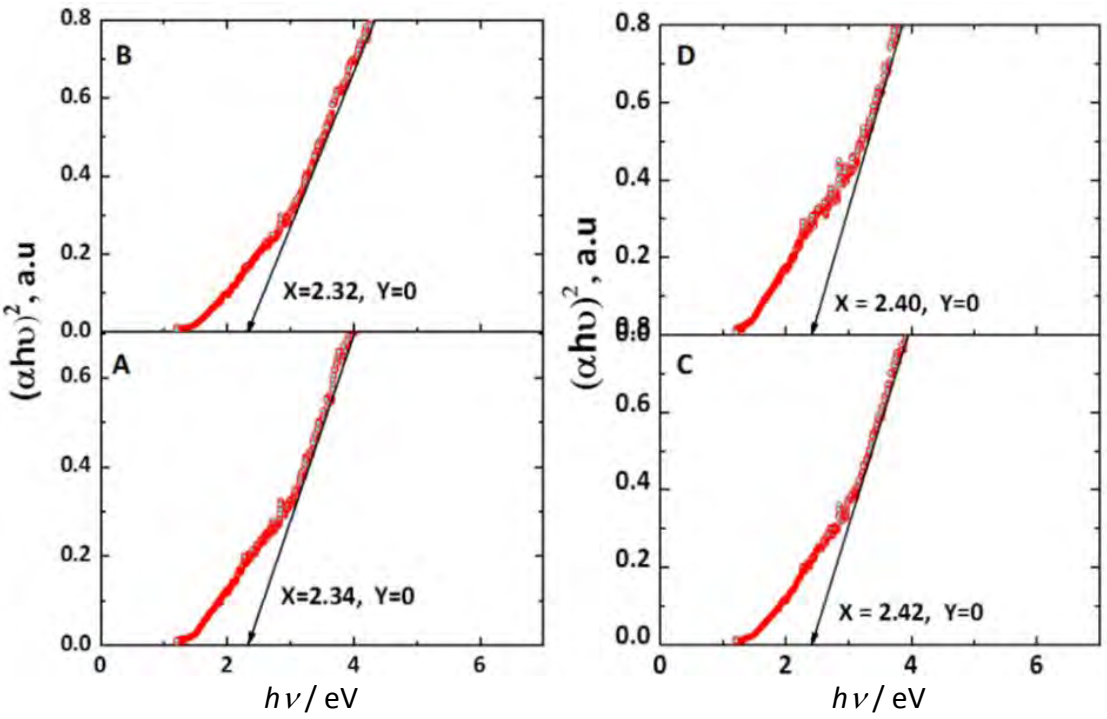

Figure 9. *Tauc plots for the evaluation of band gap of samples A) CuO/0; B) CuO/5; C) CuO/10; D) CuO/15*

Table 4. Eg *values for different ZnO and CuO NPs obtained from Tauc plot*

c (CTAB) / mM	*Eg* / eV	
	ZnO	CuO
0	3.18	2.34
5	3.19	2.32
10	3.17	2.42
15	3.18	2.40

The Tauc plots for different ZnO and CuO NPs has been presented in Fig. 8 and Fig. 9 respectively and corresponding band gap values have been summarized in Table 4. The band gap of CuO NPs increased with increase in the concentration of CTAB in the electrolytic bath during synthesis and it was found to be in between 2.32 – 2.42 eV, which is higher than that reported by Wang *et al.* [31]. However, such notable variation in the band gap of ZnO NPs was not observed. The average band gap of ZnO NP was 3.18 eV; where the literature reports a 3.2 eV band gap [3].

Photocatalytic degradation of MB dye

The photocatalytic degradation of methylene blue dye was monitored by UV-Visible spectroscopy. The variation in the absorption intensity of the methylene blue dye on UV irradiation in presence of 30 mg of ZnO NPs is presented in Fig 10.

The degradation of methylene blue was expressed in terms of % color removal by recording the changes in absorption intensity at the characteristic peak position (661 nm) in the visible region.

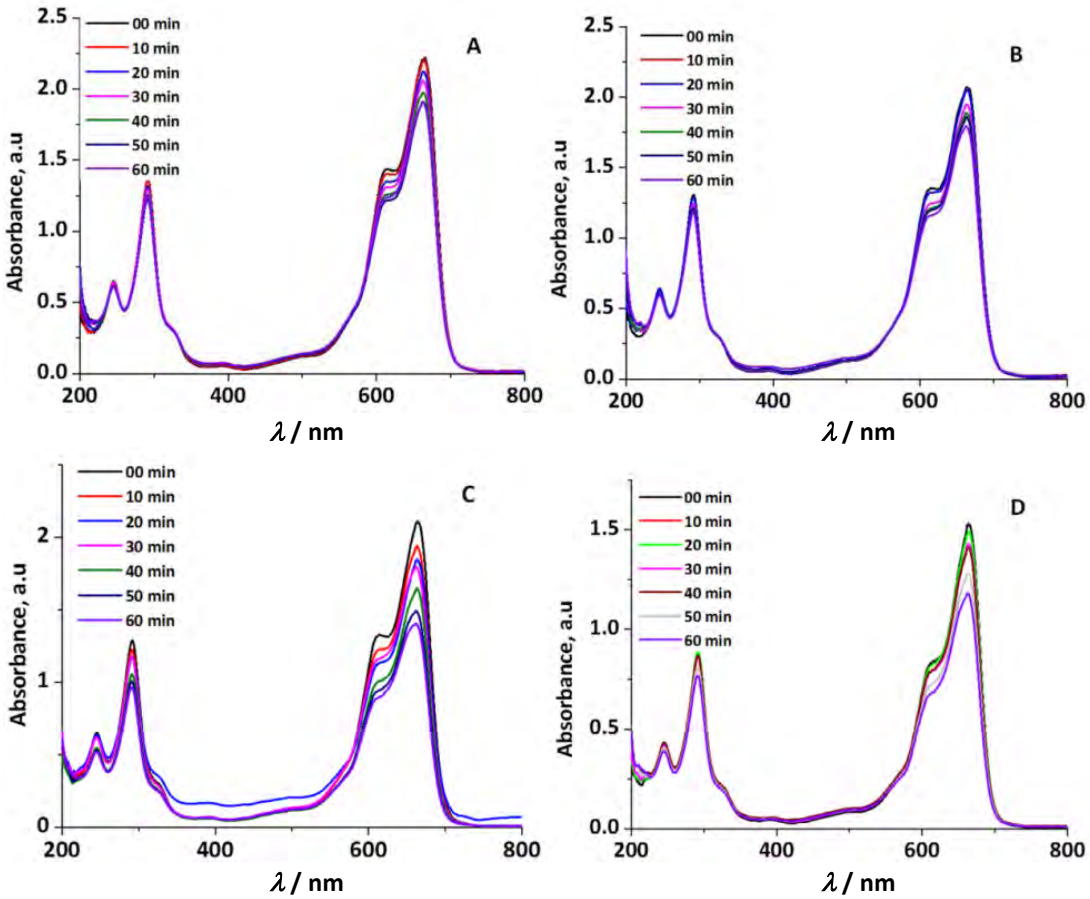

Figure 10. *The variation in the UV-Visible absorption intensity of methylene blue dye with time on electrolysis. UV irradiation in presence of 30 mg ZnO NPs; A) ZnO/0; B) ZnO/5; C) ZnO/10; D) ZnO/15*

The Eq. (3) was used to calculate the color removal:

$$\text{color removal, \%} = \frac{[A_o - A_t]}{A_o} \times 100 \quad (3)$$

where, A_o and A_t are the absorbance at 661 nm at 0 minutes and ***t*** minutes respectively. The color removal of methylene blue achieved in presence of ZnO photocatalyst was in the following order; ZnO/10 > ZnO/15 > ZnO/0 = ZnO/5. The color removal achieved after 60 minutes of UV irradiation was evaluated and given in Table 5.

Table 5: *Photocatalytic degradation of methylene blue dye*

ZnO NP	color removal, %[a]
ZnO/0	13
ZnO/5	13
ZnO/10	33
ZnO/15	22

[a] color removal achieved after 60 minutes irradiation

The CuO was also tested for its photocatalytic activity. The CuO NP under the irradiation of UV light (predominantly at 365 nm) was ineffective as a photocatalyst to degrade the MB dye. The color removal of MB achieved in presence of CuO NP and UV irradiation was insignificant.

Discussion

It is crucial to understand the mechanism of formation of ZnO and CuO in order to control their size and shape. The electrolytes used in the electrolyte bath should enhance the conductivity and assist the formation of metal hydroxides. The $NaHCO_3$ and $NaNO_3$ have been used in the synthesis of ZnO and CuO NP respectively [2-4,12]. These electrolytes facilitate the formation of metal hydroxides along with enhancing the conductivity of the electrolyte bath. The following reactions take place during the electrolysis which leads to the formation of ZnO NP in the electrolyte bath containing $NaHCO_3$ electrolyte [Eqs. (4) to (7)];

$Zn \rightarrow Zn^{2+} + 2e^-$ (on anode), E° = 0.76 V (4)

$NaHCO_3 + H_2O \rightarrow NaOH + CO_2$ (in electrolyte solution) (5)

$Zn^{2+} + 2^-OH \rightarrow Zn(OH)_2$ (in electrolyte solution) (6)

$Zn(OH)_2 \rightarrow ZnO + H_2O$ (7)

In presence of $NaNO_3$, the CuO is generated according to the following reactions [12] [Eqs. (8) to (11)];

$Cu \rightarrow Cu^{2+} + 2e^-$ (on anode), E° = 0.34 V (8)

$NO_3^- + H_2O + 2e^- \rightarrow NO_2^- + 2^-OH$ (on cathode), E° = 0.1 V (9)

$Cu^{2+} + 2^-OH \rightarrow Cu(OH)_2$ (in electrolyte solution) (10)

$Cu(OH)_2 \rightarrow CuO + H_2O$ (11)

The mechanism of NP crystal growth is usually explained as oriented aggregation in the electrolyte solution. The metal ions generated at the anode react with the ^-OH ions in the electrolyte bath to form corresponding nano-sized amorphous metal hydroxide precipitate

($Cu(OH)_2$ or $Zn(OH)_2$). A part of the precipitate undergoes dehydration to give metal oxide in the electrolyte bath (CuO or ZnO) [2-4]. However, complete conversion of all metal hydroxide into metal oxide is ensured by calcinating the sample at elevated temperatures (in this case, 300 °C). The metal oxide thus generated acts as seed for further directional aggregation of metal oxides to form precisely oriented nanostructures [12].

The advantage in electrochemical synthesis is that the precursor metal ion is slowly released from the anode metal. The current density determines the number of ions released per unit time and their availability in the electrolyte bath for further reaction. However, in chemical methods (like solvothermal and precipitation) the entire precursor metal ion is made available for reaction. The nucleation and crystal growth are the two processes which decide the particle size. If the nucleation is fast, the crystal growth is hindered and the particle size eventually remains small. These two processes occur at controlled rate in electrochemical method. The crystal growth and shape evolution is controlled by the stabilizing agent when it is present in the electrolyte bath. In this case, CTAB binds to the surface of the nuclei and prevents agglomeration or dictates the orientation of incoming species [12]. In the present study, the concentration of CTAB was more than 6 times its critical micelle concentration (CMC) *i.e.*, 0.8 mM [24]. The CTAB micelles existing at this concentration of CTAB tend to act as template for the shape evolution of NPs. The effect of CTAB concentration on the morphology and size of both ZnO and CuO NPs is clearly evident from the SEM images and the crystallite size calculated using XRD data. As mentioned earlier, from the SEM images (Fig. 3 and Fig. 4), the change in morphology of both CuO and ZnO crystals is not obvious within 5 mM CTAB. But, the tendency from regular shapes to irregular ones increased beyond the CTAB concentration ≥ 10 mM. The morphology of CuO NPs was much affected by the CTAB concentration as compared to ZnO NPs. The spindle shape of CuO NPs increased in length and gained rigidity in presence of 5 mM CTAB as noticed in the SEM images. However, when the CTAB concentration was raised to 10 mM and 15 mM, the spindle shape of CuO NPs transformed into irregular spherical shape with reduced grain size. On the other hand, the ZnO NPs retained their spherical shape irrespective of the CTAB concentration. However, the homogeneity in the shape of ZnO NPs was disrupted. The grain size of both ZnO and CuO NPs decreased with increase in CTAB concentration. From these observations, it can be deduced that the minimum concentration of CTAB required to influence the shape and size of ZnO and CuO NP crystal is ≥ 10 mM *i.e.*, more than 10 times its CMC value.

The effect of CTAB concentration on the band gap energy and absorption edge in the UV region for ZnO NPs was insignificant. However, there was a hike of 0.1 eV in the band gap of CuO NPs on increasing the concentration of CTAB from 0 mM to 15 mM. The decrease in size of CuO NPs led to the increment in band gap. The absorption edge in the UV region for CuO NPs altered with the grain size which is intern dependent on the CTAB concentration.

The influence of changes in the morphology and size of ZnO NPs reflected on its photocatalytic activity. The electrons from the valence band (VB) of ZnO NPs leap to the conduction band (CB) on UV light irradiation. Vacancies created in the valence band (holes) are represented as h_{VB}^+ and the excited electrons are given the symbol e_{CB}^-. The photogenerated positive vacancies in the VB have high oxidizing potential. These holes can react with the adsorbed water to produce hydroxyl radical and the photogenerated electrons lead to the formation of other oxidizing agents such as superoxide anions ($\cdot O_2^-$), hydrogenperoxide (H_2O_2), hydroxyl radicals ($\cdot OH$), hydrogen dioxide anion (HO_2^-) and hydroperoxy radicals ($\cdot HO_2$) as given in Eqs. (12) to (18) [7];

$$MO + h\nu \rightarrow MO\ (h_{VB}^+ + e_{CB}^-) \quad (12)$$

$$MO\ (h_{VB}^{+}) + H_2O \rightarrow MO + \cdot OH + H^{+} \quad (13)$$

$$MO\ (e_{CB}^{-}) + O_2 \rightarrow MO + \cdot O_2^{-} \quad (14)$$

$$MO\ (e_{CB}^{-}) + \cdot O_2^{-} + 2H^{+} \rightarrow MO + H_2O_2 \quad (15)$$

$$MO\ (e_{CB}^{-}) + H_2O_2 \rightarrow MO + \cdot OH + {}^{-}OH \quad (16)$$

$$O_2^{-} + H_2O_2 \rightarrow \cdot OH + {}^{-}OH + O_2 \quad (17)$$

$$O_2^{-} + H^{+} \rightarrow \cdot OH_2 \quad (18)$$

These oxidants are powerful enough to completely incinerate the organics into CO_2 and H_2O. The photocatalytic reaction efficiency increases with increase in surface area available for the adsorption of target molecule. As the size of ZnO NPs decreased with increase in CTAB concentration, the surface area available for the adsorption of dye molecules also increased. The number of MB molecules adsorbed on the ZnO/15 and ZnO/10 NPs was higher than that on ZnO/0 and ZnO/5 NPs. The % color removal of MB dye achieved after 60 minutes UV light irradiation was thus highest with ZnO/10 and ZnO/15 NPs.

Conclusion

The ZnO and CuO NPs of varying size and morphology were successfully synthesized by sacrificial anode electrochemical-thermal method. The crystallite size of both ZnO and CuO reduced with increase in concentration of CTAB in the electrolyte bath during electrolysis. The crystallite size of ZnO NPs was between 48-18 nm and for CuO it varied between 31-19 nm. The ZnO/0 and ZnO/5 NPs exhibited homogeneous size and morphology. The homogeneity of ZnO NPs was lost with increase in CTAB concentration in the electrolyte bath during electrolysis and led to the formation of irregular sized nanostructures of reduced size in presence of 10 mM and 15 mM CTAB. Similar effects were observed for the CuO NPs. The CuO NPs of uniform size and morphology were obtained in the absence of CTAB and in presence of 5 mM CTAB. The rigidity of CuO NPs enhanced in presence of 5 mM CTAB. However, on increasing the CTAB concentration to 10 mM and 15 mM the spindle shape of CuO NPs disrupted to form irregular nanostructures. The CTAB adsorbs on the surface of the metal oxide nuclei and restrains the growth of NPs by reducing the surface energy and preventing further agglomeration. CTAB tends to gain spherical structure in aqueous solution at these concentrations and act like template for the evolution of spherical NPs of irregular morphology. It can be deduced from the results that the minimum concentration of CTAB influencing the evolution of shape and size of the NP is ≥ 10 mM (greater than 10 times the CMC value of CTAB).

The effect of size and shape of ZnO NPs on the absorption edge and band gap was insignificant. The band gap of ZnO NPs lied between 3.17 – 3.19 eV. The band gap of CuO NPs showed considerable changes with size. A hike of 0.1 eV was observed due to the reduction in size of CuO NPs with increase in CTAB concentration. The photocatalytic activity of ZnO NPs was tested for the degradation of MB dye. The ZnO/10 NPs showed comparatively higher photocatalytic activity and a color removal of 33 % was achieved using this NPs with the UV light irradiation for 60 minutes.

Acknowledgement: *This work was supported by University Grants Commission, New Delhi, Govt. of India under the grant Ref: F. No. 41-231/2012 (SR) Dated 16/07/2012]; and Department of Chemistry, Kuvempu University. Authors thank Mr. Manu Kumar K N, Mr. Kiran Kumar K S and Mr. Nagaraja H N for their valuable assistance.*

References

[1] J. Song, L. Xu, C. Zhou, R. Xing, Q. Dai, D. Liu, H. Song, *Appl. Mater. Interfaces.* **5** (2013) 12928−12934.
[2] K.G. Chandrappa, T.V. Venkatesha, *J. Exper. Nanosci.* **8** (4) (2013) 516–532.
[3] K. G. Chandrappa, T. V. Venkatesha, *Nano-Micro. Lett.* **4** (1) (2012)14-24.
[4] K. G. Chandrappa, T. V. Venkatesha, K. Vathsala, C. Shivakumara, *J. Nanopart. Res.* **12** (2010) 2667–2678.
[5] H. Zhang, D. Yang, Y. Ji, X. Ma, J. Xu, D. Que, *J. Phys. Chem. B.* **108** (13) (2004) 3955-3958.
[6] F. Liu, Y. H. Leung, A. B. Djurišić, A. M. Ching, W. K. Chan, *J. Phys. Chem. C.* **117** (2013) 12218−12228.
[7] K. Kannaki, P.S. Ramesh, D. Geetha, *Int. J. Sci. Eng. Res.* **3** (9) (2012) 1-4.
[8] T. Maruyama, *Sol. Energy Mater. Sol. Cells.* **56** (1998) 85-92.
[9] Y .J. Hwang, Y. C. Ahn, H. S. Shin, C. G. Lee, G. T. Kim, H. S. Park, J. K. Lee*, Curr. Appl. Phys.* **6** (2006) 1068–1071.
[10] J. Tamaki, K. Shimanoe, Y. Yamada, Y. Yamamoto, N. Miura, N. Yamazoe, *Sens. Actuators B.* **49** (1998) 121–125.
[11] G. L. Luque, M. C. Rodrìguez, G. A. Rivas, *Talanta.* **66** (2005) 467–471.
[12] G.Q.Yuan, H.F. Jiang, C. Lin, S.J. Liao, *J. Cryst, Growth.* **303** (2007) 400–406.
[13] B. Skårman, T. Nakayama, D. Grandjean, R. E. Benfield, E. Olsson, K. Niihara, L. R. Wallenberg, *Chem. Mater.* **14** (2002) 3686-3699.
[14] S. Baruah, S. K. Pal, J. Dutta, *Nanosci. Nanotechnol-Asia.* **2** (2) (2012) 90-102.
[15] M. T. Reetz, W. Helbig, S. A. Quaiser, *Chem. Mater.* **7** (1995) 2227-2228.
[16] M. T. Reetz, W. Helbig, *J. Am. Chem. Soc.* **116** (1994) 1401-1402.
[17] M. T. Reetz, M. Winter, R. Breinbauer, T. Thurn-Albrecht, W. Vogel, *Chem. Eur. J.* **7**(5) (2001) 1084 – 1094.
[18] S. Mahamuni, K. Borgohain, B. S. Bendre, V. J. Leppert, S. H. Risbud, *J. Appl. Phys.* **85**(5) (1999) 2861-2865.
[19] M. Starowicz, B. Stypuła, *Eur. J. Inorg. Chem.* (2008) 869–872.
[20] A. B. Isaev, N. A. Zakargaeva, Z. M. Aliev, *Nanotechnol. Russia.* **6** (7–8) (2001) 463–467.
[21] P. Pandey, S. Merwyn, G. S. Agarwal, B. K. Tripathi, S. C. Pant, *J. Nanopart. Res.* **14** (2012) 709-722.
[22] M. El-Kouedi, M. L. Sandrock, C. J. Seugling, C. A. Foss, Jr, *Chem. Mater.* **10** (1998) 3287-3289.
[23] C. K. Govindappa, V. T. Venkatarangaiah, S. B. Abd Hamid, *Nano-Micro Lett.* **5**(2) (2013) 101-110.
[24] O. R. Miranda, N. R. Dollahon, T. S. Ahmadi, *Cryst. Growth Des.* **6** (12) (2006) 2747-2753.
[25] C. Bullen, P. Zijlstra, E. Bakker, M. Gu, C. Raston, *Cryst. Growth Des.* **11** (2011) 3375–3380.
[26] M. Grzelczak, J. Perez-Juste, B. Rodrıguez-Gonzalez, M. Spasova, I. Barsukov, M. Farle, L. M. Liz-Marzan*, Chem. Mater.* **20** (2008) 5399–5405.
[27] M. M. Husein, E. Rodil, J. H. Vera, *Langmuir*, **22** (2006) 2264-2272.
[28] K. S. Choi , E. M. P. Steinmiller, *Electrochim. Acta.* **53** (2008) 6953–6960.
[29] L. Ding, R. Zhang, L. Fan, *Nanoscales Res. Lett.* **8** (2013) 78.
[30] S. Valencia, J. M. Marín, G. Restrepo, *Open Mater. Sci. J.* **4** (2010) 9-14.
[31] H. Wang, J. Z. Xu, J. J. Zhu, H. Y. Che, *J. Cryst. Growth.* **244** (2002) 88–94.